

https://doi.org/10.1070/QEL17284

Influence of birefringent fibre joints on the visibility drift in a Mach–Zehnder interferometer

G.M. Krylov, O.V. Fat'yanov, A.V. Duplinskii

Abstract. **It is shown that imperfect joints of linear birefringent fibres in a fibre interferometer may result in an uncontrolled visibility drift under varying environmental conditions even with a standard phase matching device. As an example, a double Mach–Zehnder interferometer is considered, which is employed in schemes of quantum key distribution. Results of numerical simulation demonstrate the standard deviation of the quantum bit error rate (QBER), which is comparable to an average QBER value.**

Keywords: *quantum key distribution, visibility, polarisation extinction ratio, interferometer.*

1. Introduction

Presently, interferometric devices are widely used in many fields of science and technology. They are employed in machine-building [1], astronomy [2], microscopy [3], optoelectronics [4, 5], optical sensors [6–8] and in quantum optics problems including quantum key distribution (QKD) [9–12]. QKD is the technology that allows a sender (conventionally called Alice) and receiver (Bob) to safely communicate and exclude eavesdropping by a third person (Eve) [9]. The essence of QKD is the transfer of a secure crypto key by means of single elementary particles, conventionally, photons. Interferometric devices used in QKD require matching the polarisation states and phases of light beams in both arms [6, 7] for attaining a high (above 0.99) visibility of the interference pattern directly related to the quantum bit error rate (QBER) [12, 13].

For matching the polarisation states, a number of methods have been suggested, which employ polarisation controllers [14–17] and Faraday mirrors [18–20]. It is also reasonable to use linear birefringent (BF) fibres [8, 21]. An accepted method for phase matching is altering the optical path length in one of the interferometer arms. In fibre devices, this may be realised in the form of a piezoelectric actuator (fibre stretcher), which mechanically extends the fibre, thereby adjusting the phases in interferometer arms [12].

A linear BF fibre is intended for maintaining the linear polarisation of radiation [22, 23]. This fibre is characterised by strong induced birefringence due to the rotation symmetry introduced either to the refractive index profile or to stress distribution. Such a fibre possesses two orthogonal polarisation axes: 'fast' and 'slow'. If a linearly polarised (LP) radiation with the polarisation direction along any of these axes is introduced into the fibre, then it will actually propagate without changing the polarisation state. The degree of maintaining the polarisation state is determined by the polarisation extinction ratio (PER). Its typical value, for example, in the case of a widely used PANDA fibre of length 100 m is above 30 dB [24]. However, in fibre connectors the PER falls to 20 dB and less [25]. Moreover, connectors result in that at the output from just a single patch cord made of a BF fibre, the PER and polarisation state depend on the external conditions: temperature, pressure, and fibre bend [25, 26]. Hereinafter, the 'external conditions' will imply all the factors affecting the phase difference of polarisation modes in a fibre. When several BF fibres are connected in series, for example, in an interferometer, the process of energy transfer from one polarisation mode to another is easier described in the frameworks of statistical approach rather than by a complicated function of numerous time-dependent parameters [27].

The efficiency of interferometric devices made of a BF fibre was estimated numerically in [8]. An array of optical sensors presented by the parallel connection of Mach–Zehnder interferometers was simulated. The PERs of fibre connections and beam splitters were taken constant, and phase relations in the fibres varied according to various external conditions. Complementary integral distribution functions of the interference pattern visibility were determined separately for each sensor and for the array as a whole.

In the present work, a passage of optical radiation through the interferometer made of a BF fibre under varying external conditions is simulated. As an example, a double Mach–Zehnder interferometer is considered, which is used in QKD systems. For more accurate statistical description, the spread of

G.M. Krylov QRate, ul. Novaya 100, Skolkovo, 121353 Moscow, Russia; Russian Quantum Centre, Bol'shoi bulv. 30, stroenie 1, Skolkovo, 121205 Moscow, Russia; Quantum Communications Centre of NTI, National University of Science and Technology MISiS, Leninsky prosp. 4, 119049 Moscow, Russia; National Research Nuclear University MEPhI, Kashirskoe sh. 31, 115409 Moscow, Russia; e-mail: g.krylov@goqrate.com;
O.V. Fat'yanov QRate, ul. Novaya 100, Skolkovo, 121353 Moscow, Russia; Russian Quantum Centre, Bol'shoi bulv. 30, stroenie 1, Skolkovo, 121205 Moscow, Russia; Quantum Communications Centre of NTI, National University of Science and Technology MISiS, Leninsky prosp. 4, 119049 Moscow, Russia;
A.V. Duplinskii QRate, ul. Novaya 100, Skolkovo, 121353 Moscow, Russia; Russian Quantum Centre, Bol'shoi bulv. 30, stroenie 1, Skolkovo, 121205 Moscow, Russia; Quantum Communications Centre of NTI, National University of Science and Technology MISiS, Leninsky prosp. 4, 119049 Moscow, Russia; Moscow Institute of Physics and Technology (National Research University), Institutskii per. 9, 141701 Dolgoprudnyi, Moscow region, Russia

Received 21 November 2019; revision received 31 January 2020
Kvantovaya Elektronika **50** (5) 447–453 (2020)
Translated by N.A. Raspopov

the PER of beam splitters and fibre connections is taken into account. It is shown that imperfect fibre connections lead to the fluctuations of the interference pattern visibility that cannot be compensated for by a standard piezoelectric actuator. In turn, in QKD systems, visibility variations change the QBER. To our knowledge, for the first time the statistical distributions of the average QBER and standard deviation are obtained by the modelling approach, which takes into account PER dispersion in optical elements.

2. Polarisation state variation in a single patch cord

In this section and later on, the radiation is assumed monochromatic. The weakly guided mode approximation is used, where in the limiting case of equal refractive indices of the core and cladding, the longitudinal field components turn to zero, thus, leading to the plane wave approximation [28]. Also, it is assumed that fibre connectors are fabricated in the FC/APC format and, hence, have the return losses of ~ 60 dB, which excludes noticeable contributions from the effects related to mutual reflections between elements. This gives a chance to employ Jones calculus for describing the evolution of the polarisation state in a fibre [29].

Consider propagation of a plane wave in a single patch cord made of a BF fibre. As mentioned, if the LP radiation with the polarisation oriented along any of the fibre axes is introduced, then it will actually propagate without changing its polarisation state. Nevertheless, when BF fibres are connected, there is always a small misalignment angle α_1.

If the polarisation vector of radiation makes an angle α_1 (Fig. 1) with a fibre polarisation axis, then the input wave can be presented as a vector sum of two orthogonal components, each propagating with a particular velocity in the fibre due to a difference in the refraction indices. The greater part of radiation passes along the initially prescribed axis, whereas the smaller part propagates normally to it. In this case, the PER will be related to the misalignment angle by the relationship [25]:

$$K = 10\lg(1/\tan^2\alpha_1). \tag{1}$$

The Jones matrix describing an input connector corresponds to the matrix of rotation by a misalignment angle α_1:

$$R(\alpha_1) = \begin{pmatrix} \cos\alpha_1 & -\sin\alpha_1 \\ \sin\alpha_1 & \cos\alpha_1 \end{pmatrix}. \tag{2}$$

When radiation propagates in a BF fibre, the orthogonal polarisation modes acquire a phase difference φ due to the difference in the refractive indices. This phase delay is also affected by temperature, pressure, and fibre bends. The phase difference φ can hardly be controlled because it instantaneously varies in time. In this part of patch cord, birefringence is described by the Jones matrix

$$B = F\begin{pmatrix} \exp\left(\frac{\mathrm{i}}{2}\varphi\right) & 0 \\ 0 & \exp\left(-\frac{\mathrm{i}}{2}\varphi\right) \end{pmatrix}, \tag{3}$$

where F is the factor determined by the phase incursion common for both the axes. In further calculations, this factor will be neglected since it does not affect the polarisation state.

Radiation propagates in a fibre to the output connector, which is characterised by a misalignment angle α_2; each of the orthogonal components splits into two components. The resulting interference determines the PER and depends on the phase difference φ, which varies in time. If we assume that the input light wave is polarised along the slow axis, then the result of passing it through the patch cord is described by the polarisation state vector

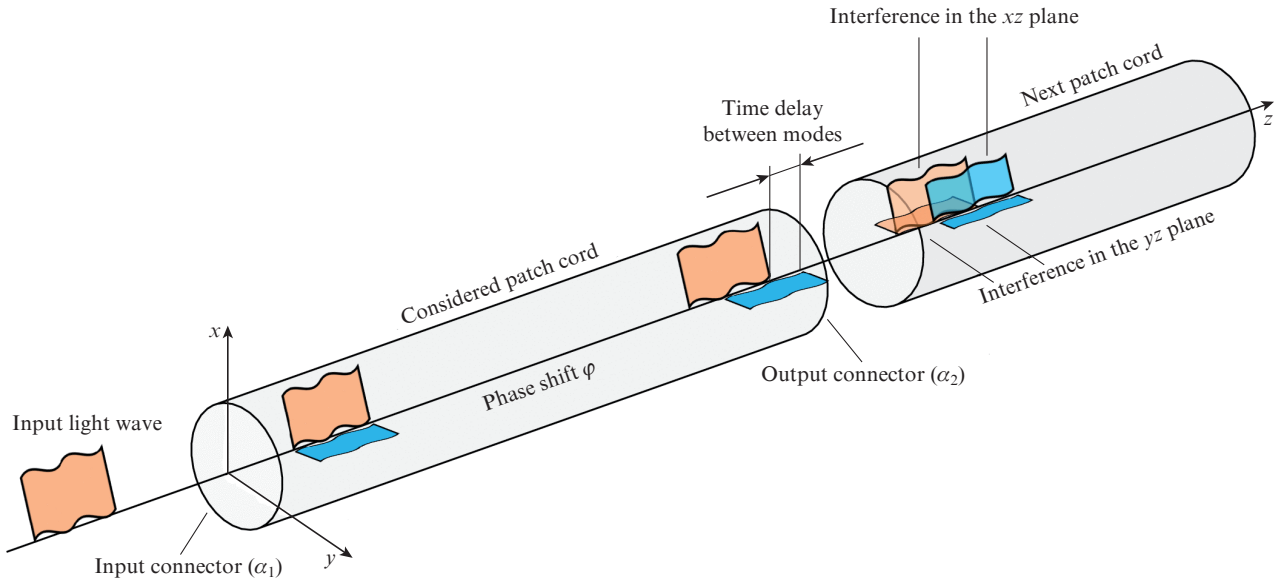

Figure 1. Propagation of a light wave through a patch cord made of a BF fibre. At the input connection, it splits into two waves polarised along the fibre axes. Due to a difference in the refractive indices in the BF fibre, the waves propagate at different velocities. Then at the output connector, each of them splits again into two waves. The waves polarised along similar directions interfere pairwise at the input to the next patch cord. Here, x is the slow axis, y is the fast axis, and z is the propagation direction.

$$\boldsymbol{P} = R(\alpha_2)B(\lambda)R(\alpha_1)\begin{pmatrix}1\\0\end{pmatrix}. \tag{4}$$

It was shown in [26] that the dependence of the result of interference on φ, and, consequently, on the radiation wavelength λ in certain conditions leads to light pulse distortion; however, for monochromatic radiation these effects are insignificant.

3. Radiation propagation in an interferometer made of a BF fibre

Consider propagation of optical radiation through an interferometer. A high interference contrast requires maintaining a constant phase difference in the arms and equal polarisation transformations for the paths covered by the interfering radiation. The first condition can be fulfilled by using a phase matching device, for example, a piezoelectric actuator. The second condition can be fulfilled by assembling an interferometer from a BF fibre. A schematic of such an interferometer is presented in Fig. 2.

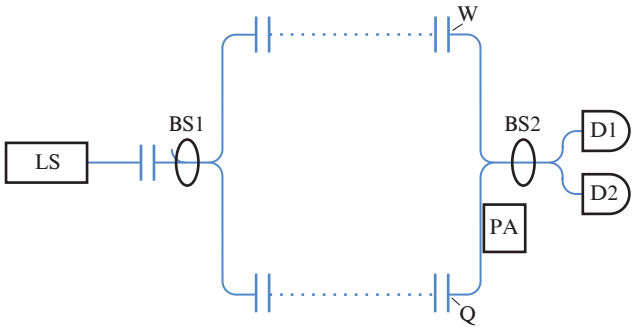

Figure 2. Schematic of the interferometer made of a BF fibre: (LS) laser source; (BS1, BS2) polarisation-maintaining fibre beam splitters 50/50; (PA) piezoelectric actuator; (D1, D2) detectors; vertical double lines mark fibre joints.

An output polarisation-maintaining beam splitter BS2 has two input arms with two orthogonal eigenmodes in each of them. Thus, evolution of the polarisation state is described by a 4×4 matrix. The states are determined by the vector

$$\boldsymbol{A} = \begin{pmatrix}A_{\mathrm{s}}^{(1)}\\A_{\mathrm{f}}^{(1)}\\A_{\mathrm{s}}^{(2)}\\A_{\mathrm{f}}^{(2)}\end{pmatrix}, \tag{5}$$

where the superscript corresponds to the bottom (1) or top (2) arm, and subscript corresponds to the slow (s) or fast (f) fibre axis.

The present work takes into account the final PER for the polarisation maintaining fibre beam splitters. The BS2 action can be described by the product of two matrices 4×4: the matrix C_{id} corresponding to an ideal beam splitter 50/50 and rotation matrix C_{rot} [8]:

$$C_{\mathrm{id}} = \frac{1}{\sqrt{2}}\begin{pmatrix}1&0&\mathrm{i}&0\\0&1&0&\mathrm{i}\\\mathrm{i}&0&1&0\\0&\mathrm{i}&0&1\end{pmatrix}, \tag{6}$$

$$C_{\mathrm{rot}} = \begin{pmatrix}\cos\alpha_{\mathrm{bs}}&-\sin\alpha_{\mathrm{bs}}&0&0\\\sin\alpha_{\mathrm{bs}}&\cos\alpha_{\mathrm{bs}}&0&0\\0&0&\cos\alpha_{\mathrm{bs}}&-\sin\alpha_{\mathrm{bs}}\\0&0&\sin\alpha_{\mathrm{bs}}&\cos\alpha_{\mathrm{bs}}\end{pmatrix}, \tag{7}$$

where α_{bs} is the angle that determines the PER fall. Below, we will show that the matrix C_{rot} does not affect visibility. Consequently,the matrix C_{id} is sufficient for modelling BS2.

For simplicity, in the interferometer part preceding BS2, the polarisation is described by a 2×2 matrix. For this purpose, one should consider each arm separately. The polarisation states in the bottom and top arms are determined, respectively, by the Jones vectors:

$$\boldsymbol{A}^{(1)} = \begin{pmatrix}A_{\mathrm{s}}^{(1)}\\A_{\mathrm{f}}^{(1)}\end{pmatrix} \text{ and } \boldsymbol{A}^{(2)} = \begin{pmatrix}A_{\mathrm{s}}^{(2)}\\A_{\mathrm{f}}^{(2)}\end{pmatrix}.$$

Rotation and birefringence matrices for the jth patch cord in the kth arm ($k = 1, 2$) can be presented in the form

$$R_j^{(k)} = \begin{pmatrix}\cos\alpha_j^{(k)}&-\sin\alpha_j^{(k)}\\\sin\alpha_j^{(k)}&\cos\alpha_j^{(k)}\end{pmatrix}, \tag{8}$$

$$B_j^{(k)} = \begin{pmatrix}\exp\left(\frac{\mathrm{i}}{2}\varphi_j^{(k)}\right)&0\\0&\exp\left(-\frac{\mathrm{i}}{2}\varphi_j^{(k)}\right)\end{pmatrix}. \tag{9}$$

BS1 has a single bottom arm; hence, the initial state for the upper arm is empty:

$$\boldsymbol{A}_{\mathrm{in}}^{(2)} = \begin{pmatrix}0\\0\end{pmatrix}.$$

The initial state for the bottom arm is a wave with the polarisation along the slow axis:

$$\boldsymbol{A}_{\mathrm{in}}^{(1)} = \begin{pmatrix}\sqrt{I_0}\\0\end{pmatrix},$$

where I_0 is the sum intensity. For the bottom and top interferometer arms, the Jones matrices for BS1 can be presented, respectively, as follows:

$$C^{(1)} = \frac{1}{\sqrt{2}}\begin{pmatrix}\cos\alpha_{\mathrm{bs}}&-\sin\alpha_{\mathrm{bs}}\\\sin\alpha_{\mathrm{bs}}&\cos\alpha_{\mathrm{bs}}\end{pmatrix}\begin{pmatrix}1&0\\0&1\end{pmatrix} = \frac{1}{\sqrt{2}}R_{\mathrm{bs}}D^{(1)}, \tag{10}$$

$$C^{(2)} = \frac{1}{\sqrt{2}}\begin{pmatrix}\cos\alpha_{\mathrm{bs}}&-\sin\alpha_{\mathrm{bs}}\\\sin\alpha_{\mathrm{bs}}&\cos\alpha_{\mathrm{bs}}\end{pmatrix}\begin{pmatrix}\mathrm{i}&0\\0&\mathrm{i}\end{pmatrix} = \frac{1}{\sqrt{2}}R_{\mathrm{bs}}D^{(2)}. \tag{11}$$

The fibre section connected to a laser source and the section between BS2 and detectors (Fig. 2) are insignificant for analysis and are therefore neglected.

As mentioned, the interferometer part preceding BS2 is described by 2×2 matrices. For the intermediate Jones vectors corresponding to the bottom and top arms one can write the expressions

$$\boldsymbol{A}_{\mathrm{int}}^{(1)} = B_{n+1}^{(1)}\left(\Pi_{j=1}^{n}T_j^{(1)}\right)C^{(1)}B_0^{(1)}R_0^{(1)}\boldsymbol{A}_{\mathrm{in}}^{(1)}, \tag{12}$$

$$\boldsymbol{A}_{\mathrm{int}}^{(2)} = B_{m+1}^{(2)}\left(\Pi_{j=1}^{m}T_j^{(2)}\right)C^{(2)}B_0^{(2)}R_0^{(2)}\boldsymbol{A}_{\mathrm{in}}^{(1)}, \tag{13}$$

where $T_j^{(k)} = R_j^{(k)} B_j^{(k)}$.

For obtaining the final vector of states $\boldsymbol{A}_{\text{out}}$ one should compose a four-component vector $\boldsymbol{A}_{\text{int}}$ from (12) and (13) and then affect it by the matrix for BS2:

$$\boldsymbol{A}_{\text{int}} = \begin{pmatrix} \boldsymbol{A}_{\text{int}}^{(1)} \\ \boldsymbol{A}_{\text{int}}^{(2)} \end{pmatrix}, \tag{14}$$

$$\boldsymbol{A}_{\text{out}} = C_{\text{id}} \boldsymbol{A}_{\text{int}}. \tag{15}$$

For estimating the interference pattern quality, the parameter is introduced, which is called visibility and determined by the formula

$$V = \frac{I_{\max} - I_{\min}}{I_{\max} + I_{\min}}, \tag{16}$$

where $I_{\max}$ and $I_{\min}$ are the maximal and minimal radiation intensities in the interferometer output arms. For analysing phenomenologically the processes related to visibility, one can assume the beam splitter BS2 to be ideal, that is, it can be modelled by the matrix C_{id}. Indeed, its action is considered as that of an ideal beam splitter, which is accompanied by a reduction of PER. The PER fall [see (7)] changes the polarisation state only inside each of the arms (but not between those), which does not affect the output intensity and, consequently, visibility of the interference pattern.

While passing through the interferometer comprised of a BF fibre and the patch cords connected in series, each making its own contribution dependent on time and external conditions into the PER reduction, the light wave gradually goes to a polarisation mode initially not intended for propagation. In BS2, fast modes interfere with fast, and slow modes interfere with slow. This construction can be considered as two independent interferometers: 'fast' and 'slow'. A result of the interference depends on the phase difference and determines the intensity in each of the output arms, which directly affects visibility. The piezoelectric actuator (Fig. 2) is aimed at affecting the fibre section in such a way that the phase difference induced in two input arms of BS2 would provide the maximal visibility. The latter is attained in the case, where the result of interference in the slow interferometer (either constructive or destructive) in any of the output arms coincides with the result of interference in the fast interferometer in the same arm. For example, if both the interferometers yield constructive interference in the top arm and destructive in the bottom arm then the upper arm will concentrate the maximal power and the bottom arm will concentrate the minimal power. Thus, visibility becomes maximal. A piezoelectric actuator, which slightly varies the fibre length, actually identically changes the optical path length along both fast and slow axes, not substantially changing the resulting polarisation state [30]. However, for reaching the maximal visibility, it is necessary to affect the fibre in such a way that the optical path lengths along both the axes will vary independently, because the phase differences in the interferometer arms corresponding to the fast and slow axes vary differently depending on external conditions. It follows that a standard piezoelectric actuator can only partially compensate for a variation of the interferometer visibility.

The action of the piezoelectric actuator was modelled as follows. It was assumed that it similarly affects the phases of fast and slow components introducing a common phase φ_{piezo}. This assumption is rather well realised in real conditions at slight fibre extensions [30]. The matrix $B_{n+1}^{(1)}$ responsible for the fibre section, where the piezoelectric actuator is placed, can be presented in the form:

$$B_{n+1}^{(1)} = \begin{pmatrix} \exp\left[\mathrm{i}\left(\varphi_{\text{piezo}} + \frac{1}{2}\varphi_{n+1}^{(1)}\right)\right] & 0 \\ 0 & \exp\left[\mathrm{i}\left(\varphi_{\text{piezo}} - \frac{1}{2}\varphi_{n+1}^{(1)}\right)\right] \end{pmatrix}. \tag{17}$$

Hence, the vector is

$$\boldsymbol{A}_{\text{int}} = \begin{pmatrix} M_{\text{s}}^{(1)} \exp\left[\mathrm{i}\left(\varphi_{\text{piezo}} + \frac{1}{2}\psi_{n+1}^{(1)}\right)\right] \\ M_{\text{f}}^{(1)} \exp\left[\mathrm{i}\left(\varphi_{\text{piezo}} - \frac{1}{2}\psi_{n+1}^{(1)}\right)\right] \\ M_{\text{s}}^{(2)} \exp\left(\frac{\mathrm{i}}{2}\psi_{m+1}^{(2)}\right) \\ M_{\text{f}}^{(2)} \exp\left(-\frac{\mathrm{i}}{2}\psi_{m+1}^{(2)}\right) \end{pmatrix}, \tag{18}$$

where $M_{\text{s,f}}^{(k)}$ are the absolute values of complex amplitudes $A_{\text{s,f}}^{(k)}$ at points W and Q (Fig. 2), and $\psi_{n+1}^{(1)}$ and $\psi_{m+1}^{(2)}$ depend on $\varphi_{n+1}^{(1)}$ and $\varphi_{m+1}^{(2)}$ and on the phase difference of complex amplitudes $A_{\text{s}}^{(k)}$ and $A_{\text{f}}^{(k)}$ ($k = 1, 2$). Common phases of amplitudes $A_{\text{s}}^{(k)}$ and $A_{\text{f}}^{(k)}$ were neglected by the same reason as the factor F in (3) was. Output amplitudes $\boldsymbol{A}_{\text{out}}$ were calculated by formula (15). Without loss of generality, it was assumed that the radiation with intensity $I_{\max}$ arises in the bottom arm and $I_{\min}$ corresponds to the top arm. Accordingly, we have [31]

$$I_{\max} = \max_{0 \leqslant \varphi_{\text{piezo}} < 2\pi} (I_{\text{s out}}^{(1)} + I_{\text{f out}}^{(1)}) = \max_{0 \leqslant \varphi_{\text{piezo}} < 2\pi} \left\{ \frac{I_0}{2} \right.$$

$$+ \sqrt{(M_{\text{s}}^{(1)} M_{\text{s}}^{(2)})^2 + (M_{\text{f}}^{(1)} M_{\text{f}}^{(2)})^2 + 2 M_{\text{s}}^{(1)} M_{\text{s}}^{(2)} M_{\text{f}}^{(1)} M_{\text{f}}^{(2)} \cos(\Delta\psi)}$$

$$\left. \times \cos\left[\varphi_{\text{piezo}} + f\left(M_{\text{s,f}}^{(1,2)}, \psi_{n+1}^{(1)}, \psi_{m+1}^{(2)}\right)\right] \right\}, \tag{19}$$

where $I_{\text{s out}}^{(k)}$ and $I_{\text{f out}}^{(k)}$ are the intensities at BS2 output; $(M_{\text{s}}^{(1)})^2 + (M_{\text{f}}^{(1)})^2 + (M_{\text{s}}^{(2)})^2 + (M_{\text{f}}^{(2)})^2 = I_0$; and $\Delta\psi = \psi_{n+1}^{(1)} - \psi_{m+1}^{(2)}$. The maximization condition is fulfilled when $\varphi_{\text{piezo}} = 2\pi l - f(M_{\text{s,f}}^{(1,2)}, \psi_{n+1}^{(1)}, \psi_{m+1}^{(2)})$, $l \in \mathbb{Z}$. In this case, the visibility is

$$V = \frac{2}{I_0} \times$$

$$\times \sqrt{(M_{\text{s}}^{(1)} M_{\text{s}}^{(2)})^2 + (M_{\text{f}}^{(1)} M_{\text{f}}^{(2)})^2 + 2 M_{\text{s}}^{(1)} M_{\text{s}}^{(2)} M_{\text{f}}^{(1)} M_{\text{f}}^{(2)} \cos(\Delta\psi)}. \tag{20}$$

This value can be qualitatively interpreted as the characteristic of a mismatch between the interference patterns for fast and slow interferometers, which prevents forming of a common interference pattern.

4. Results of numerical simulation

In 1992, Ch. Bennett suggested a phase coding scheme, namely, a double Mach–Zehnder interferometer, which is now quite popular [10]. It comprises two unbalanced interferometers, one for Alice and the other for Bob, connected by an optical fibre. The key is coded as a phase difference of interfering pulses. A scheme of the interferometer made of a BF

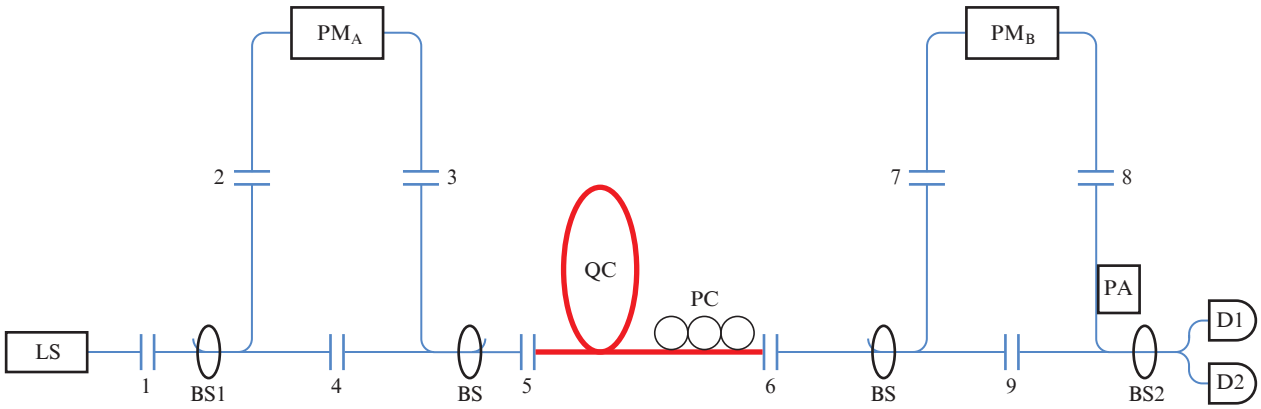

Figure 3. Double Mach–Zehnder interferometer: (LS) laser source; (PM_A, PM_B) Alice and Bob phase modulators; (QC) quantum channel; (PC) polarisation controller; (BS, BS1, BS2) polarisation-maintaining fibre beam splitters 50/50; (PA) piezoelectric actuator; thin lines show BF fibre; bold lines indicate standard single-mode optical fibre; (D1, D2) detectors; digits enumerate fibre joints.

fibre is presented in Fig. 3. Later we will show that for analysing propagation of radiation in such interferometer one can use a simplified scheme shown in Fig. 2.

When input pulses are counted on Bob's side, three peaks are observed in the time domain: the earliest peak corresponds to photons that have passed through the 'short–short' arms, the second corresponds to the 'short–long' and 'long–short' arms, and the last relates to the 'long–long' arms. The first and third peaks refer to noninterfering pulses, whereas the second corresponds to interfering pulses [9].

In analysis, it is convenient to represent the system as a Mach–Zehnder interferometer (Fig. 4). This presentation is possible because the pulses interesting from the viewpoint of key distribution (that have passed through 'short–long' and 'long–short' arms) are time-separated and interfere only on the last fibre beam splitter 50/50; at intermediate splitters the interference is absent. This fact, in addition to the requirement of a small pulse spectral width relative to its centre wavelength (is fulfilled in real installations), allows one to transfer from considering pulses to a monochromatic light wave.

In fibre QKD schemes, lithium niobate electro-optical phase modulators are widely employed due to a fast response [32–34]. It is assumed that the fast and slow crystal axes in modulators are parallel to fibre axes and their polarisation mode dispersion and polarisation-dependent losses are negligible; thus, modulators do not reduce the PER. The quantum channel comprises a standard single-mode optical fibre; therefore, the polarisation state does not turn on the 5th joint and is neglected in the modelling. Dispersion effects in the quantum channel are assumed negligible and neglected from the consideration as well. It is also assumed that a polarisation controller is installed at the end of the quantum channel, which transfers the radiation polarisation for optimal input into connector 6, however, with a small error. Thus, connector 6 is modelled by a rotation matrix, which is the same for both the arms. The intermediate light splitters are modelled only by rotation matrices R_{bs} because in the present analysis the combining and splitting properties are insignificant.

Thus, the scheme of the modelled interferometer is simplified to the diagram shown in Fig. 2. All above equations are applicable; however, now I_0 in formula (19) is the sum intensity of interfering waves, that is, the waves propagating in the paths 'short–long' and 'long–short' of the interferometer arms. The interferometer visibility corresponds to the optical QBER (hereinafter, it is designated by E). The calculation is performed by the formula [9]:

$$E = \frac{1 - V}{2}. \tag{21}$$

MATLAB software was used for modelling the evolution of the polarisation state in radiation passage through the double Mach–Zehnder interferometer. In addition, changes in visibility were calculated depending on external conditions. The modelling was realised basing on numerical experiments, presented by sets of simulations. It is assumed that in each of the numerical experiments, the connector misalignment angles $\alpha_j^{(k)}$ and parameters α_{bs} are constant (but random), and the phase differences $\varphi_j^{(k)}$ uniformly distributed over interval $[0, 2\pi)$ vary from simulation to simulation. This corresponds to considering a single particular Mach–Zehnder interferometer under varying external conditions. In each experiment, the values of $\alpha_j^{(k)}$ and α_{bs} satisfy normal distribution conditions with the standard deviations 5° and 3.5°, respectively [26]. Thus, an ensemble of numerical experiments defines a sample of various interferometers, each of those being in varying external conditions.

In each simulation, the phase differences $\varphi_j^{(k)}$ were chosen basing on the statistical distribution, then the field amplitudes $A_{s,f}^{(1,2)}$ were calculated at points Q and W just after the 8th and 9th joints (Fig. 4). Then parameters V (20) and E (21) were found, and the calculation passed on to next simulation. Totally, 10^4 numerical experiments have been performed each comprising 10^4 simulations for configurations with five joints in the arms (Fig. 4) and the same number of simulations for configurations with 6 and 7 joints. In this way, the contribution of the number of joints into the reduction of interference pattern visibility was estimated.

Figure 5 presents the distribution functions for an average QBER $\langle E \rangle$ and its standard deviation $\sigma(E)$ in various interferometer configurations versus the number of joints. Averaging the $\langle E \rangle$ value over all interferometers yields the values of 2.35%, 2.69%, and 3.04% (is denoted as $\langle E \rangle_{av}$), and averaging $\sigma(E)$ yields 2.11%, 2.45%, and 2.76% [is denoted as $\sigma_{av}(E)$] for five, six, and seven joints, respectively. Thus, the QBER spread in the considered cases is actually comparable

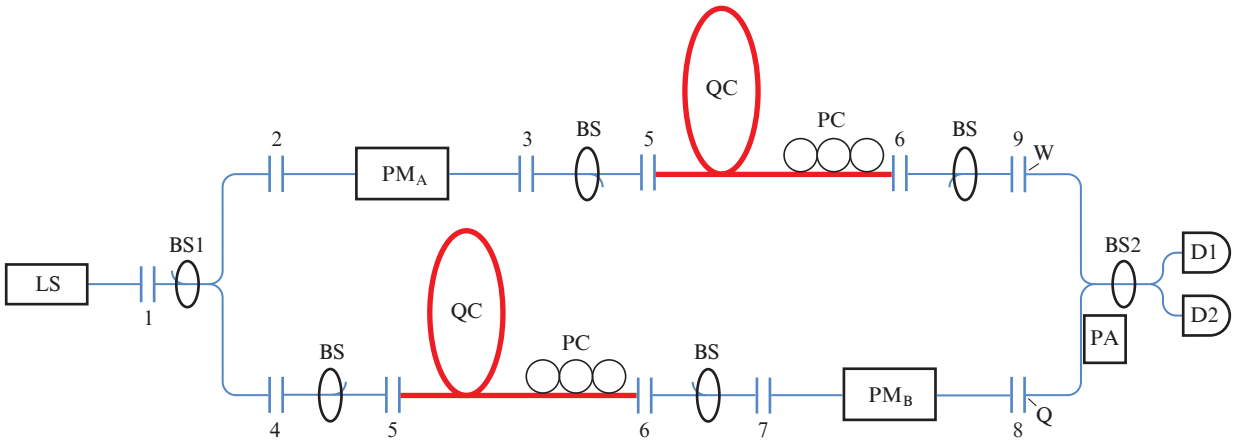

Figure 4. Double Mach–Zehnder interferometer used in the simulation: (LS) laser source; (PM_A, PM_B) Alice and Bob phase modulators; (QC) quantum channel; (PC) polarisation controller; (BS, BS1, BS2) polarisation-maintaining fibre light splitters 50/50; (PA) piezoelectric actuator; thin lines show BF fibre; bold lines indicate standard single-mode optical fibre; (D1, D2) detectors; digits enumerate fibre joints.

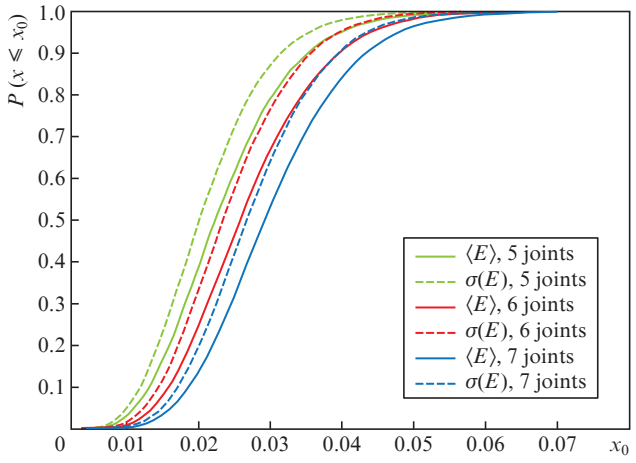

Figure 5. (Colour online) Distribution functions for the average QBER $\langle E \rangle$ and standard QBER deviation $\sigma(E)$ for interferometer configurations with five, six, and seven joints in each arm. Here, $x = \langle E \rangle$, $\sigma(E)$.

to its average value. $\langle E \rangle_{av}$ and $\sigma_{av}(E)$ grow with the number of joints. Consequently, the QBER can substantially change in the process of key exchange.

5. Conclusions

Numerical modelling is performed for light monochromatic wave passage through a Mach–Zehnder interferometer made of a BF fibre. A double interferometer used in QKD systems is considered as an example. It is shown that a standard phase adjusting piezoelectric actuator exhibits a drift of the interferometer visibility, which finally affects the QKD error rate. Statistical characteristics of the visibility and QBER for several interferometer configurations differing in the number of joints are obtained by numerical modelling. For each configuration, a set of various interferometers was considered differing in the fabrication quality of fibre joints and light splitters. In turn, each interferometer from the set was modelled with various external conditions. The QBER averaged over interferometers and over external conditions, and the standard QBER deviation averaged over interferometers grow with the number of joints. In this case, the QBER deviation is comparable on the order of magnitude to its average value: $\langle E \rangle_{av}$ = 2.35%, 2.69%, 3.04% and $\sigma_{av}(E)$ = 2.11%, 2.45%, 2.76% for five, six, and seven joints, respectively. Data obtained testify a substantial influence of the quality and number of joints in a BF fibre on the drift of the QBER under external conditions despite of the presence of a feedback device.

In future, we plan to analyse propagation of optical pulses in interferometers taking into account effects pertaining to medium dispersion properties and depolarisation of radiation.

Acknowledgements. The authors are grateful to D.V. Sych for useful advice and constructive discussions.

The work was supported by the Russian Scientific Foundation (Grant No. 17-71-20146).

References

1. Kolomiitsov Yu.V. *Interferometry. Osnovy inzhenernoi teorii* (Interferometers. Fundamentals of Engineering Theory) (Leningrad: Mashinostroenie, 1976).
2. Akhmanov S.A., Nikitin S.Yu. *Physical Optics* (Oxford: Clarendon Press, 1997; Moscow: Izd. MSU, Nauka, 2004).
3. Dyson J. *Proc. R. Soc. London, Ser. A*, **204** (1077), 170 (1950).
4. Wooten E.L., Kissa K.M., Yi-Yan A., Murphy E.J., Lafaw D.A., Hallemeier P.F., et al. *IEEE J. Sel. Top. Quantum Electron.*, **6** (1), 69 (2000).
5. Mahmoud M., Bottenfield C., Cai L., Piazza G. *Proc. 30th Annual Conf. IEEE Photonics Society* (Orlando, USA, 2017) p.223.
6. Stowe D.W., Moore D.R., Priest R.G. *IEEE Trans. Microwave Theory Tech.*, **30** (10), 1632 (1982).
7. Kersey A.D., Dandridge A., Tveten A.B. *Opt. Lett.*, **13** (4), 288 (1988).
8. Tur M., Boger Y.S., Shaw H.J. *J. Lightwave Technol.*, **13** (7), 1269 (1995).
9. Gisin N., Ribordy G., Tittel W., Zbinden H. *Rev. Mod. Phys.*, **74** (1), 145 (2002).
10. Bennett C.H. *Phys. Rev. Lett.*, **68** (21), 3121 (1992).
11. Townsend P.D., Rarity J.G., Tapster P.R. *Electron. Lett.*, **29** (14), 1291 (1993).
12. Gobby C., Yuan Z.L., Shields A.J. *Appl. Phys. Lett.*, **84** (19), 3762 (2004).
13. Dušek M., Haderka O., Hendrych M., Myška R. *Phys. Rev. A*, **60** (1), 149 (1999).
14. Okoshi T. *IEEE Trans. Electron Devices*, **32** (12), 2624 (1985).
15. Lefevre H.C. *Electron. Lett.*, **16** (20), 778 (1980).
16. Ulrich R. *Appl. Phys. Lett.*, **35** (11), 840 (1979).

17. Walker N.G., Walker G.R. *Electron. Lett.*, **23** (6), 290 (1987).
18. Mo X.F., Zhu B., Han Z.F., Gui Y.Z., Guo G.C. *Opt. Lett.*, **30** (19), 2632 (2005).
19. Muller A., Herzog T., Huttner B., Tittel W., Zbinden H., Gisin N. *Appl. Phys. Lett.*, **70** (7), 793 (1997).
20. Martinelli M. *Opt. Commun.*, **72** (6), 341 (1989).
21. Hu Y.-M., Chen Z., Meng Z., Zhang X., Song Z. *Chin. J. Lasers*, **24**, 891 (1997).
22. Noda J., Okamoto K., Sasaki Y. *J. Lightwave Technol.*, **4** (8), 1071 (1986).
23. Sears F.M. *J. Lightwave Technol.*, **8** (5), 684 (1990).
24. Sasaki Y. et al. *J. Lightwave Technol.*, **4** (8), 1097 (1986).
25. Penninckx D., Beck N. *Appl. Opt.*, **44** (36), 7773 (2005).
26. Penninckx D., Beck N., Gleyze J.F., Videau L. *J. Lightwave Technol.*, **24** (11), 4197 (2006).
27. Monerie M. *Appl. Opt.*, **20** (14), 2400 (1981).
28. Gloge D. *Appl. Opt.*, **10** (10), 2252 (1971).
29. Jones R.C. *J. Opt. Soc. Am.*, **38** (8), 671 (1948).
30. Zhang F., Lit J.W. *Appl. Opt.*, **32** (13), 2213 (1993).
31. Oo N., Gan W.S. *Int. J. Computer Commun. Eng.*, **1** (3), 200 (2012).
32. Marand C., Townsend P.D. *Opt. Lett.*, **20** (16), 1695 (1995).
33. Duplinskiy A., Ustimchik V., Kanapin A., Kurochkin Y. *Proc. Int. Conf. Micro- and Nano-Electronics 2016* (Zvenigorod, Russia, 2016) Vol. 10224, p. 102242W.
34. Duplinskiy A., Ustimchik V., Kanapin A., Kurochkin V., Kurochkin Y. *Opt. Express*, **25** (23), 28886 (2017).